Journal of Physics and Chemistry of Solids 136 (2020) 109016

Contents lists available at ScienceDirect

Journal of Physics and Chemistry of Solids

journal homepage: www.elsevier.com/locate/jpcs

Optical properties and birefringence of $ZnIn_2S_4$ layered crystals

I.G. Stamov[a], V.V. Zalamai[b], N.N. Syrbu[b,*], A.V. Tiron[b]

[a] T.G. Shevchenko State University of Pridnestrovie, 25 Oktyabrya Street 107, 3300, Tiraspol, Republic of Moldova
[b] Technical University of Moldova, 168 Stefan cel Mare Avenue, 2004, Chisinau, Republic of Moldova

ARTICLE INFO

Keywords:
Interference spectra
Birefringence
Frenkel excitons
Refractive indices
Band structure

ABSTRACT

Interference spectra of layered $ZnIn_2S_4$ crystals were investigated for samples of different thicknesses (7.5–900 μm). Spectral dependences of refractive indices (n^a and n^b) for light waves with different polarizations were calculated and their intersection observed at energy $E_0 \sim 2.38$ eV. The refractive indices difference ($\Delta n = n^a - n^b$) was determined at energy range 0.8–3.0 eV. Features observed in reflection and absorption spectra were attributed to the band-to-band electron transitions at $k = 0$. Magnitudes of valence bands (V_1, V_2 and V_3, V_4) splitting due to crystal field and spin–orbital interaction were determined. Electron transitions in energy interval 2–6 eV were identified on the basis of available theoretical band structure calculations.

1. Introduction

Crystals of $ZnIn_2S_4$ are triple $A^{II}B_2^{III}C_4^{VI}$ semiconductor compounds and attract interest due to their pronounced layered structure [1–8]. The crystals are photosensitive and luminescent and possess interesting optical properties [8–10]. Its various crystalline polytypes (α, β and γ) are of particular interest [11,12]. Crystals are of interest from a technological point of view and chemical methods have shown the possibility of producing thin nano-layers [12–17]. Electron band structure calculations improve understanding of the optical, photoelectrical and luminescent properties of these materials [11,12,18].

Photocatalytic water splitting has been intensely investigated for solar to hydrogen conversion. For example TiO_2 was used by Fujishima and Honda [19] as a photoanode to split water into H_2 and O_2 in a photoelectrochemical cell. Many wide band-gap semiconductors have been explored as active elements for photocatalytic water splitting and some have achieved high quantum yields under ultraviolet irradiation [20]. At the same time, semiconducting photocatalysts, which are active for H_2 production under visible light irradiation, must be developed in order to efficiently utilize solar energy. Thus, much effort has focused on the development of visible-light-driven photocatalysts [20]. Due to its wide band gap, $ZnIn_2S_4$ can be used as a photocatalyst active with ultraviolet light irradiation [10]. This, in turn, requires a more detailed and comprehensive study of optical properties of this material.

The present work involves an investigation of interference spectra anisotropy for $ZnIn_2S_4$ crystals in a wide energy diapason (0.8–3 eV). Spectral dependences of refractive indices (n_a(E||a) and n_b(E||b)) and their intersection at energy $E_0 \sim 2.38$ eV were determined. Band-to-band electron transitions in $k = 0$ were revealed using reflection and absorption spectra. The magnitudes of valence band (V_1, V_2 and V_3, V_4) splitting due to crystal field (Δ_{cf}) and spin–orbital interaction (Δ_{so}) in the Brillouin zone center were estimated. Optical functions (n, k, ε_1 and ε_2) in the region of electron transitions were calculated and discussed in the framework of theoretical band structure calculations.

2. Experimental methods

The $ZnIn_2S_4$ single crystals were grown by the gas transport method. The obtained crystals had dimensions of 2 cm × 2 cm and thicknesses from a few microns to 1 mm. The crystals of R_{3m}-C_{3v}^5 symmetry are red-yellow plates and have been attributed to polytype α. Another type of crystal is of similar size but with a lighter yellow color and have been attributed to the R_{3m}-D_{3d}^5 symmetry (polytype γ) and to the R_{3m}^1-C_{3v}^1 symmetry (polytype β) [11,12,18]. The structure of the single crystal was controlled by X-ray diffraction (XRD). The XRD spectra of $ZnIn_2S_4$ crystals are shown in Fig. 1, and the inset illustrates an image of investigated samples.

Low-temperature optical spectra of crystals deposited in a closed helium LTS-22C 330 optical cryogenic system were measured by MDR-2 spectrometer (USSR LOMO) with luminosity 1:2 and linear dispersion 0.7 nm/mm. Photoluminescence measurements were carried out on a DFS-32 double spectrometer (USSR LOMO) with luminosity 1:5 and linear dispersion 0.5 nm/mm and on a SDL-1 double high-aperture spectrometer (USSR LOMO) with optical efficiency 1:2 and linear dispersion 0.7 nm/mm. Most measurements were performed when entrance and exit spectrometer slits did not exceed 70 μm, i.e. with

* Corresponding author.
E-mail address: sirbunn@yahoo.com (N.N. Syrbu).

https://doi.org/10.1016/j.jpcs.2019.05.013
Received 11 December 2018; Received in revised form 8 May 2019; Accepted 9 May 2019
Available online 10 May 2019

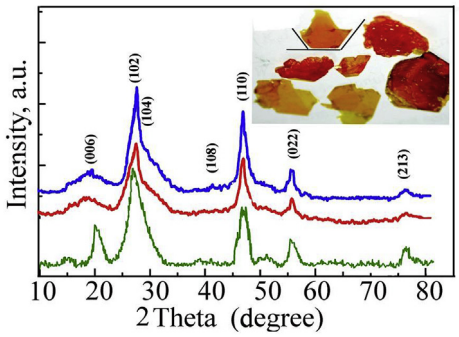

Fig. 1. XRD spectra of $ZnIn_2S_4$ crystals. Inset shows crystal image.

resolution of ~0.5 meV.

3. Results and discussion

Crystals of $ZnIn_2S_4$ are amazing objects for optical transmission (absorption) spectra measurements because they are layered and with weak bonds between layers. These weak bonds allow receiving from the gas phase very thin plates of thicknesses around tens of nanometers.

The absorption spectra (***K***) of $ZnIn_2S_4$ crystals of different thicknesses (***d*** ~ 50–900 μm) measured at temperatures 10, 60 and 300 K, and a unit cell with ***a***, ***b*** and ***c*** axes directions are shown in Fig. 2A. The temperature coefficient of absorption edge shift is equal to 0.02 eV/K. The ***K*** of 67 μm crystal and the reflection spectrum (***R***) of 845-μm thick crystal measured at room temperature is shown in Fig. 2B. Pronounced interference was observed at energies less than 2.5 eV. Four bands were observed in the ***K*** of thin crystals: ***f1***, 2.567 eV; ***f2***, 2.598 eV; ***f1′***, 2.728 eV; and ***f2′***, 2.765 eV. These bands were also found in the ***R*** of thick samples where negligible transparency occurred. These bands appeared in ***R*** energies of 2.591, 2.628, 2.728 and 2.765 for ***f1***, ***f2***, ***f1′*** and ***f2′***, respectively. Amplitudes of ***f1*** and ***f2*** reflectivity bands (distance between maximum and minimum of respective band) were 2–2.5%. Energy splitting of bands ***f1***(***f1′***) and ***f2***(***f2′***) was 37 meV and distance between ***f1***(***f2***) and ***f1′***(***f2′***) was 137 meV. Received data had good consistency with previous findings [4–7].

Vaipolin et al. [7] investigated spectral dependences of quantum efficiency of In–$ZnIn_2S_4$ surface-barrier structures and found photosensitivity maxima at 2.35–2.6 and 2.88–3.1 eV. They found exponential growth of photosensitivity at $E > 2.7$ eV and a shoulder due to band-to-band electron transitions at 2.88 eV. An "absolute" maximum at 3.1 eV occurred in their photosensitivity spectra and the photosensitivity changed from 2 to 0.8 at 3.1 and 2.5 eV, respectively [7].

General theory of optical phenomenon in semiconductors indicates that direct electron transitions are observed in reflection spectra. Since the discussed transitions were found in reflection and absorption spectra, we assumed that they were due to impurity or Frenkel exciton states, as in the case of $PbGa_2S_4$ crystals [19]. We speculate that bands ***f1*** and ***f2*** were caused by the ground state (n = 1) and bands ***f1′*** and ***f2′*** by the excited state (n = 2) of Frenkel excitons. In this case, the Rydberg constant ***R*** is of the order of 220 meV and, by virtue of this, these bands could be detected at room temperature. It is possible that these maxima were all related to the ground states and reflect the complex structure of valence bands in $\boldsymbol{k} = 0$. The small magnitude of reflectivity change (2–2.5%) was caused by weak bonds between layers of $ZnIn_2S_4$ crystal structure.

Interference in reflection and transmission spectra was observed in transparency region of thin crystals (***d*** ~ 1–50 μm), i.e. at E < 2.7 eV. The transmission spectra (T) of crystals measured at 10 K in E⊥c, E||a (V) and E⊥c, E||b (G) polarizations and in unpolarized light (n/p) are shown in Fig. 3. Transmission spectra (T*) were also measured for crystal deposition between crossed polarizers (V-G). A feature at 2.3 eV (***δ***) was observed in interference spectra at all polarizations (Fig. 3). Amplitude of interference fringes for all polarizations decreased at energy of 2.3 eV (marked by ***δ***). This feature was pronounced at 10 K and very weak at 300 K. Such a feature is also observed in all birefractive crystals because refractive indices differ for light waves that are polarized parallel and perpendicular to the anisotropy axis [19,20]. The examined crystals had cleavage faces perpendicular to the ***c*** axis. Most likely the ***δ*** feature was due to diverse refractive indices for E||b and E||a polarizations.

Investigation of birefringence dispersion in $CdGa_2S_4$ crystals by the polarized light-beam interference method showed that spectral dependences of refractive indices differed for ***E***||***c*** ($\boldsymbol{n_o}$) and ***E***⊥***c*** ($\boldsymbol{n_e}$) polarizations [20]. The spectral dependences of abovementioned refractive indices intersect at $\boldsymbol{\lambda_o}$ wavelength ($\boldsymbol{\lambda_o}$ = 485.6 nm [20]), known as the isotropic wavelength. Spectral dependence of $\Delta\boldsymbol{n} = \boldsymbol{n_e} - \boldsymbol{n_o}$ has a zero value (intersect X-axis) at wavelength $\boldsymbol{\lambda_o}$. The birefringence changes sign when crossing the value $\boldsymbol{\lambda_o}$, i.e. crystal goes from optically positive for $\boldsymbol{\lambda} < \boldsymbol{\lambda_o}$ to optically negative for $\boldsymbol{\lambda} > \boldsymbol{\lambda_o}$.

The interference transmission spectra of 1.9-μm thick $ZnIn_2S_4$ crystals in crossed polarizers at 10 K are shown in Fig. 3. Fabry–Perot interference overlaps with the birefringence phenomenon in crystals of these thicknesses. This is because at $\boldsymbol{\lambda_o}$ the phase difference between two mutually perpendicularly polarized modes propagating in the

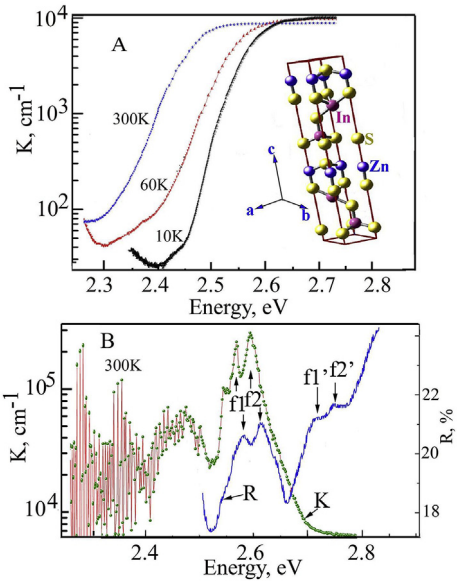

Fig. 2. A – Absorption (***K***) spectra measured at temperatures 10, 60 and 300 K; inset shows a unit cell of $ZnIn_2S_4$ polytype with $\boldsymbol{C_{3v}^5}$ symmetry. B–***K*** and reflection (R) spectra measured at room temperature.

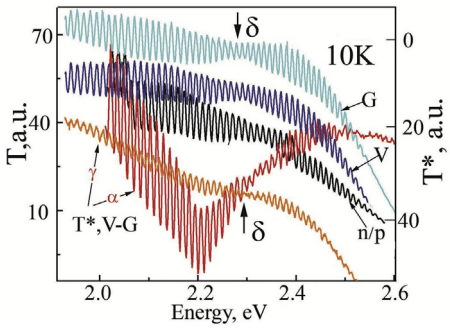

Fig. 3. Transmission spectra (***T***) of $ZnIn_2S_4$ crystals in E||a (V) and E||b (G) polarizations, in unpolarized light (n/p) and in crossed polarizers (V–G) measured at 10 K.

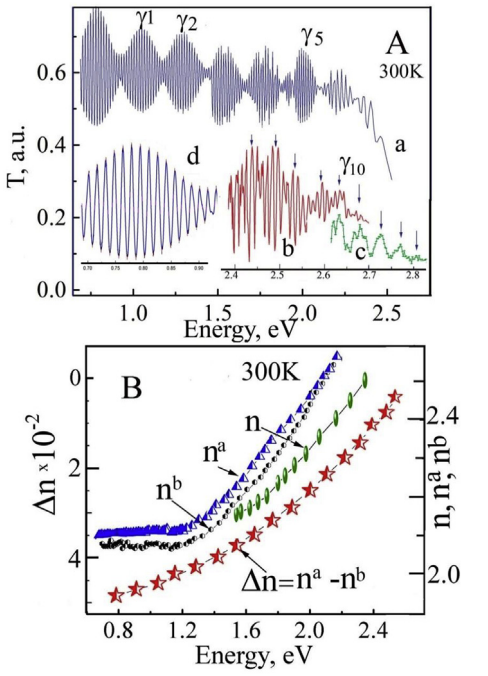

Fig. 4. A – Transmission spectra of $ZnIn_2S_4$ crystals of (a, d) 47, (b) 27 and (c) 17 μm thicknesses measured at temperature 300 K. B – Spectral dependences of refractive indices in polarizations $\boldsymbol{E}||\boldsymbol{a}$ ($\boldsymbol{n}^a$), $\boldsymbol{E}||\boldsymbol{b}$ ($\boldsymbol{n}^b$) and in unpolarized light ($\boldsymbol{n}$) and refractive indices difference $\Delta\boldsymbol{n} = \boldsymbol{n}^a - \boldsymbol{n}^b$.

crystal is always equal to zero. Therefore, in the interference spectrum of birefringence at $\boldsymbol{\lambda_0}$, either the full maximum (with parallel polarizers) or the zero minimum (with crossed polarizers) is observed.

Transmittance of crystals in crossed polarizers depends on thickness and on the refractive indices difference ($\Delta\boldsymbol{n} = \boldsymbol{n}^a(\boldsymbol{E}||\boldsymbol{a}) - \boldsymbol{n}^b(\boldsymbol{E}||\boldsymbol{b})$). Increasing of T* and decreasing of interference fringe intensity (marked as feature $\boldsymbol{\delta}$) despite the small thickness of crystal occurred in transmission spectra of the system. This system consists of two crossed polarizers and a birefractive $ZnIn_2S_4$ crystal deposited between them.

Transmission spectra of crystals of different thicknesses were measured for calculation of refractive indices dependences. The transmission spectra of crystals of 47 μm measured at temperature 300 K are shown in Fig. 4A(a). The thin structure of Fabry–Perot interference grouped into fringe packages (marked as $\gamma\boldsymbol{1}$, $\gamma\boldsymbol{2}$ etc.) was evident. Measured experimental transmission interference was worked up using a corresponding mathematical program, which determined maxima and minima positions. The spectral dependence of refractive index was calculated from energy positions of determined maxima (minima) using the following relationship [21]:

$$n = \frac{M}{2d\left(\frac{1}{\lambda_1} - \frac{1}{\lambda_2}\right)} \quad (1)$$

where $\boldsymbol{M} = 1$ for neighboring maxima (minima) $\boldsymbol{\lambda_1}$ and $\boldsymbol{\lambda_2}$ in interference spectra.

Spectral dependences of refractive indices $\boldsymbol{n}^a$ for $\boldsymbol{E}||\boldsymbol{a}$ polarization, $\boldsymbol{n}^b$ for $\boldsymbol{E}||\boldsymbol{b}$ polarization and n for the unpolarized case are shown in Fig. 4B. Spectral dependences of refractive indices difference ($\Delta\boldsymbol{n} = \boldsymbol{n}^a - \boldsymbol{n}^b$) were determined from interference fringe packets marked $\gamma\boldsymbol{1}$, $\gamma\boldsymbol{2}$ etc. Refractive indices $\boldsymbol{n}^a$ and $\boldsymbol{n}^b$ at temperature 300 K rose with increasing energy and were practically equal at ~2.2–2.3 eV. This was confirmed by calculated values of $\Delta\boldsymbol{n}$ whose minimum value was also in this energy region.

Spectral dependences of refractive indices in polarized and unpolarized light ($\boldsymbol{n}$) and refractive indices differences ($\Delta\boldsymbol{n}^*$, $\Delta\boldsymbol{n} = \boldsymbol{n}^a - \boldsymbol{n}^b$) calculated from transmission spectra measured at 10 K are shown in

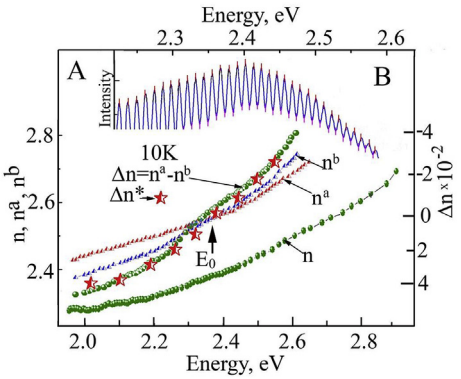

Fig. 5. Spectral dependences of refractive indices in unpolarized light ($\boldsymbol{n}$) and in $\boldsymbol{E}||\boldsymbol{a}$ ($\boldsymbol{n}^a$) and $\boldsymbol{E}||\boldsymbol{b}$ ($\boldsymbol{n}^b$) polarizations and refractive indices differences $\Delta\boldsymbol{n}^*$, $\Delta\boldsymbol{n}$ for $ZnIn_2S_4$ crystals at 10 K. Inset shows a result of interference maximums position determination.

Fig. 5. The inset shows the result of interference maxima position determinations (position of extremes marked by red dashes) (Fig. 5B). Spectral dependence $\Delta\boldsymbol{n}^*$ was calculated from energy position of interference fringe packets ($\gamma\boldsymbol{1}$, $\gamma\boldsymbol{2}$, etc.; Fig. 4) observed in interval 2–2.6 eV for crystals of different thicknesses (Fig. 5). The $\Delta\boldsymbol{n}$ magnitude was determined as difference $\boldsymbol{n}^a - \boldsymbol{n}^b$. The value of $\Delta\boldsymbol{n}$ at 10 K was positive for $\boldsymbol{E} < 2.38$ eV and negative for $\boldsymbol{E} > 2.38$ eV (Fig. 5). Changes of $\Delta\boldsymbol{n}$ determined from Fabry–Perot interference and from birefringence interference were practically the same (Fig. 5).

The $\boldsymbol{A}$ and $\boldsymbol{B}$ maxima at energies 2.851 and 2.892 eV were observed in absorption spectra of $ZnIn_2S_4$ crystals of 12 μm thickness measured at temperatures 10, 20 and 30 K (Fig. 6). Absorption spectra of 12-μm thick crystals and the reflection spectrum of 7.5-μm sample measured at 10 K are presented for comparison in Fig. 6B. Broad bands were found at energies 2.872 and 2.905 eV in absorption spectra and were shown in the reflection spectrum at similar energies. The interference fringes were laid over the main band contours. Splitting of $\boldsymbol{A}$ and $\boldsymbol{B}$ bands was

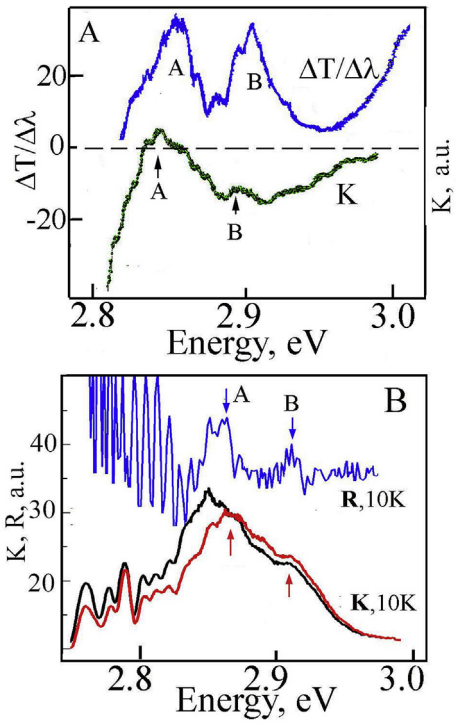

Fig. 6. Absorption ($\boldsymbol{K}$), reflection ($\boldsymbol{R}$) and wavelength modulated transmission spectra of $ZnIn_2S_4$ crystals measured at low temperatures.

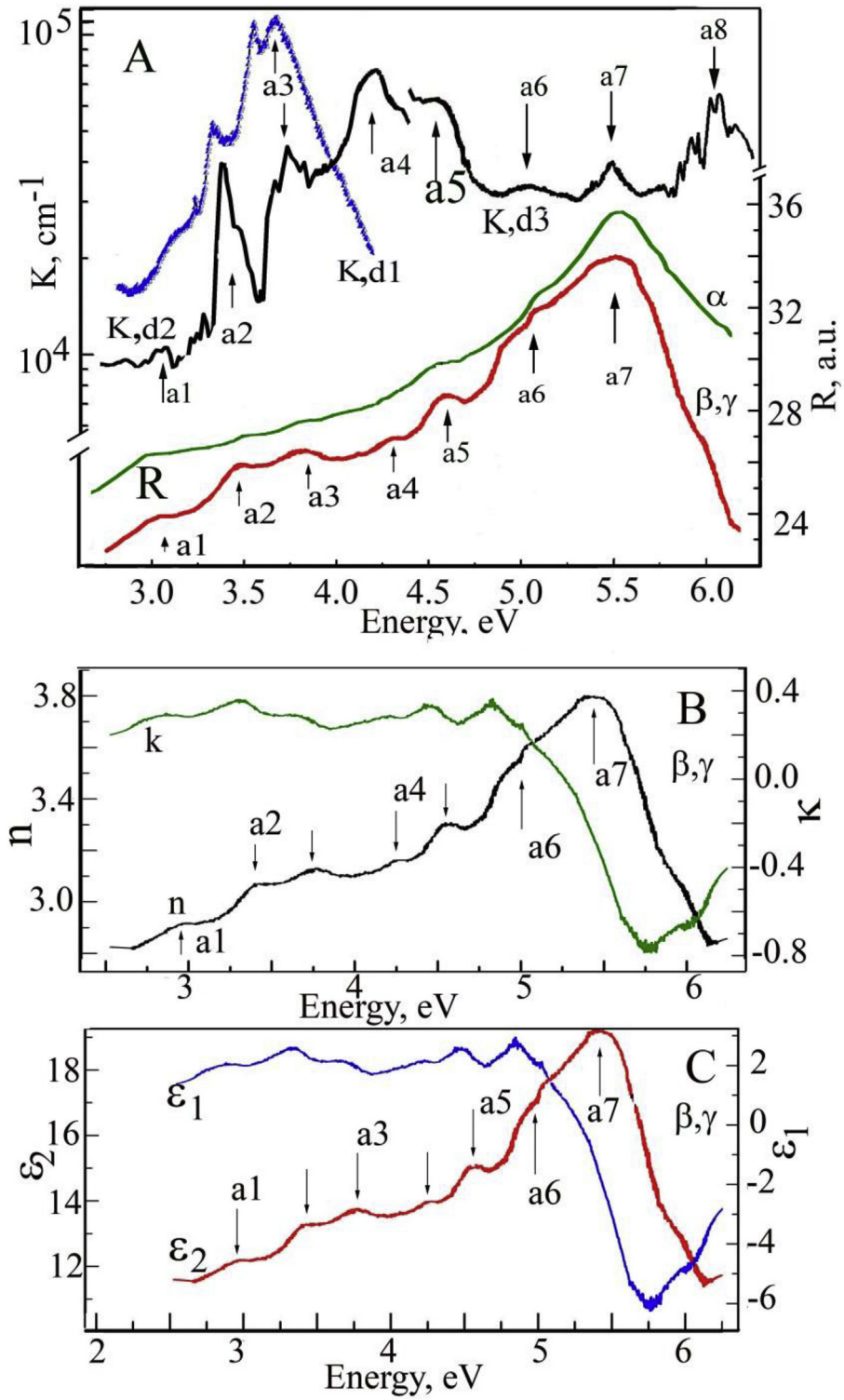

Fig. 7. A – Absorption (***K***) spectra of $ZnIn_2S_4$ nanocrystals with different thicknesses (***d1***, ***d2*** and ***d3***: 620, 540 and 210 nm, respectively) and reflection (***R***) spectra of thick crystal (1.1 mm) measured at 300 K. B, C – Spectral dependences of refractive index (***n***), extinction coefficient (***κ***), real (ε_1) and imaginary (ε_2) parts of permittivity.

equal to 38 meV.

Absorption bands at energies 3.055 (***a1***), 3.305 (***a2***), 3.404 (***a3***) and 3.759–3.777 eV (***a4***) were observed in absorption spectra of $ZnIn_2S_4$ nanocrystals of 620 (***d1***) and 540 nm (***d2***) thicknesses (Fig. 7). Weak features in the absorption spectrum of a thinner sample (210 nm ***d3***) were found at energies 4.541, 4.774, 5.165 and 5.573 eV for ***a4–a7***, respectively. Reflection spectra in the intrinsic region (2–6 eV) measured on thick crystal (d ~ 1.1 mm) contained reflection maxima (a1–a7) at energies coinciding with those from absorption spectra (Fig. 7 and Table 1). These reflection maxima in the intrinsic absorption region were caused by direct electron transitions between valence and conduction bands.

Theoretical calculations of band structure were carried out by pseudopotential method for ***α***, ***β*** and γ polytypes of $ZnIn_2S_4$ with C_{3v}^5,

Table 1
Energy positons of absorption and reflection spectra maximums and corresponding electron transitions.

Ind.	Absorption, eV		Reflectivity, eV			Transitions
	300 K	10 K	300 K	10 K	300 K [11]	
A		2.806		2.806		$\Gamma(V_1) \longrightarrow \Gamma(C_1)$
B		2.851		2.845		$\Gamma(V_2) \longrightarrow \Gamma(C_1)$
a1	3.055	3.029	3.03		2.96	$\Gamma(V_3) \longrightarrow \Gamma(C_1)$
a2	3.404		3.425		3.56	$\Gamma(V_1,V_2) \longrightarrow \Gamma(C_2)$
a3	3.548		3.763			$\Gamma(V_3) \longrightarrow \Gamma(C_2)$
	3.779					$\Gamma(V_4) \longrightarrow \Gamma(C_2)$
a4	4.615		4.278		4.7	$\Gamma(V_3,V_4) \longrightarrow \Gamma(C_3)$
a5	5.165		4.563		5.1	$\Gamma(V_1,V_2) \longrightarrow \Gamma(C_4)$
						$\Gamma(V_3,V_4) \longrightarrow \Gamma(C_4)$
a6	5.573		5.06		5.7	$A\text{-}S(V_2) \longrightarrow A\text{-}S(C_1)$
a7	5.548		5.573			$\Gamma(V_3) \longrightarrow \Gamma(C_2)$
						$\Gamma(V_4) \longrightarrow \Gamma(C_2)$

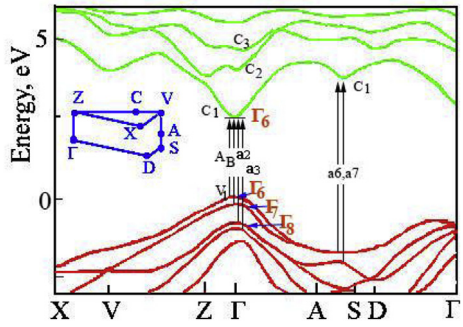

Fig. 8. Central part of the band structure for $ZnIn_2S_4$ crystals according to previously published results [18].

C_{3v}^1 and D_{3d}^3 symmetries, respectively. Theoretical calculations of the band structure for symmetries C_{3v}^1 (polytype ***β***) and D_{3d}^3 (polytype γ) were very similar. There were also previous mentions of an interesting difference between phases ***β*** and γ and phase ***α*** of C_{3v}^5 symmetry [11,12]. The main element of all $ZnIn_2S_4$ polytypes is a packet consisting of seven atomic layers (S–Zn–S–In_Ω–S–In_τ–S, where Ω and τ are indexes indicating octahedral and tetrahedral structures, respectively). The packing number in cells and arrangement of sulfur layers differ among the various polytypes.

Band structure calculations for $ZnIn_2S_4$ show that extremes of valence and conduction bands determining minimal band gap lies in the Γ point of the Brillouin zone [10,11]. The band structure theoretical calculations for $ZnIn_2S_4$ crystals were carried out for actual points of the Brillouin zone (***X***, ***V***, ***Z***, Γ, ***A***, ***S*** and ***D***) [11,12]. Yousaf et al. [18] performed theoretical calculations of band structure for $ZnIn_2S_4$ and $HgIn_2S_4$ crystals and for other actual points of the Brillouin zone (***W***, ***L*** and ***K***). According to our calculation the minimum band gap was also localized in the Brillouin zone center. The valence band maxima were recognized as weak in theoretical calculations; however, it should be noted that our results agree with earlier data [11,12].

Theoretical calculations of the energy band structure in the vicinity of all abovementioned points of the Brillouin zone were performed without taking into account spin–orbital interaction and crystal field. Valence bands in these points, according to the approaches of theoretical calculations, were degenerated. Reduction of crystal lattice symmetry from chalcopyrite to C_{3v}^5, C_{3v}^1 and D_{3d}^3 symmetries leads to band splitting due to the crystal field. A spin–orbital interaction also results in band splitting. As a result, the degenerated bands split onto elementary bands (Fig. 8).

The maxima of reflection and absorption spectra ***f1*** and ***f2*** (Fig. 2) were observed in $ZnIn_2S_4$ crystals in the band-gap minimum localized in $\boldsymbol{k} = 0$ in $\boldsymbol{E} \perp \boldsymbol{c}$ polarization. These features were probably caused by transitions from Frenkel's exciton levels. Maxima ***f1′*** and ***f2′*** were due to Frenkel's excitons formed by valence bands V_3 and V_4 and conduction band C_1. In this case, for ***α*** polytype, top valence band V_1 and V_2 splitting was equal to 37 meV. Valence bands V_3 and V_4 were split on the same value. The splitting value between pairs of bands V_1, V_2 and V_3, V_4 was 137 meV. For ***β*** polytype crystals, maxima in reflection and absorption spectra in energy diapason 2.6–2.8 eV were not observed. Only maxima ***A*** and ***B*** splitting on 38 meV were discovered in reflection and absorption spectra of ***β*** polytype crystals (Fig. 6). These features were due to direct electron transitions between pairs of bands V_1, V_2 and band C_1. For this polytype, the valence bands V_3 and V_4 split on 38 mV and energy distance between bands V_2 and V_3 was 185 meV.

Thereby the difference in band gap energy for polytypes exists but is not essential. The interband minimum was less for ***α*** than for ***β*** and γ polytypes. The magnitudes of bands splitting for different polytypes differed only slightly. The maxima were found out at higher energies ($E > 3.1$ eV) both in reflection and absorption spectra (Fig. 7). Reflection and transmission spectra of ***β*** and γ polytypes and reflection spectra of ***α*** polytype are shown in Fig. 7. It was not possible to select nanocrystals for measuring absorption in the high-energy region for ***α*** polytype as was made for ***β*** and γ polytypes.

Reflection spectra in the region of fundamental electron transitions for ***α***, ***β*** and γ polytypes had similar contours and features. Maxima were observed at the same energies; however, in ***β*** and γ polytypes the maxima were more pronounced (Fig. 7). Using spectral dependences of measured reflectivity, the spectral dependences of the optical constants (n, κ, ε_1 and ε_2) were calculated using Kramers–Kronig relations (Fig. 7B and C).

As mentioned above, the features in absorption and reflection spectra (***f1***, ***f2***, ***f1′*** and ***f2′***) discovered in ***α*** polytypes and maxima (A and B) in ***β*** and γ polytypes were due to direct electron transitions in the Brillouin zone center from the valence bands V_1–V_4 to conduction band C_1. Theoretical calculations of the band structure for these crystals revealed the presence of valence and conduction band extrema at the same values of wave vectors mainly in the center of the Brillouin zone ($\boldsymbol{k} = 0$) and in the ***A–S*** direction (Fig. 8). Based on these data, the maxima of reflection spectra ***a1*** and ***a3*** were caused by electron transitions in the Brillouin zone center from valence bands V_1–V_4 to conduction band C_2 (Fig. 8 and Table 1). The maxima a4, a5 and a6 were probably due to transitions from the V_1–V_4 bands to the C_3 and C_4 bands (Table 1).

4. Conclusions

The refractive indices n^a ($\boldsymbol{E}||\boldsymbol{a}$) and n^b ($\boldsymbol{E}||\boldsymbol{b}$) at room and low temperatures were calculated from interference spectra of $ZnIn_2S_4$ crystals. At temperature 10 K, these refractive indices intersected at $E_0 \sim 2.38$ in an isotropic point. In the energy range 0.8–3.0 eV, the spectral dependence of the refractive indices difference ($\Delta n = n^a - n^b$) was calculated. The band-to-band electron transitions in $\boldsymbol{k} = 0$ were revealed in the reflection and absorption spectra and the V_1, V_2 and V_3, V_4 valence band splitting was determined. The valence bands V_3 and V_4 split by 38 mV and the energy distance between bands V_2 and V_3 was 185 meV. The electron transitions in the energy interval of 2–6 eV were identified using actual theoretical band structure calculations.

References

[1] N.A. Goryunova, Compound Diamond-like Semiconductors, Moskow, Sov. Radio, 1968.
[2] YuA. Valov, A.A. Lebedev, K. Ovezov, V.D. Prochukhan, YuV. Rud, Sov. Tech. Phys. Lett. 2 (1976) 410.
[3] A.A. Lebedev, P.N. Metlinsky, YuV. Rud, V.G. Tyrzyu, Sov. Phys. Semiconduct. 11 (1977) 1038.
[4] A.N. Georgobiani, S.I. Radautsan, N.M. Tighinyanu, Sov. Phys. Semiconduct. 19 (1985) 193.
[5] R.N. Bekmimbetov, YuV. Rud, M.A. Tairov, Sov. Phys. Semiconduct. 21 (1987) 1051.

[6] A.A. Vaipolin, YuA. Nikolaev, V.Yu Rud, YuV. Rud, E.I. Terukov, N. Fernelius, Semiconductors 37 (2) (2003) 187.
[7] Y. Xia, Q. Li, K. Lv, M. Li, Appl. Surf. Sci. 398 (2017) 81.
[8] Y. Xia, Q. Li, K. Lv, D. Tang, M. Li, Appl. Catal., B 206 (2017) 344.
[9] Sh Shen, P. Guo, L. Zhao, Yu Du, L. Guo, J. Solid State Chem. 184 (2011) 2250.
[10] A. Anede, L. Cugusi, E. Grilli, M. Guzzi, F. Raga, A. Spiga, Solid State Commun. 29 (1979) 829.
[11] F. Aimerich, F. Meloni, G. Mula, Solid State Commun. 29 (1979) 235.
[12] Y. Xie, Yu Liu, H. Cui, W. Zhao, Ch Yang, F. Huang, J. Power Sources 265 (2014) 62.
[13] Wen-Hui Yuan, Zi-Long Xia, Li Li, Chin. Chem. Lett. 24 (2013) 984.
[14] Y. Chen, Sh Hu, W. Liu, X. Chen, L. Wu, X. Wang, P. Liu, Zh Li, Dalton Trans. 40 (2011) 2607.
[15] Kong-Wei Cheng, Chao-Ming Huang, Ya-Chien Yu, Chun-Ting Li, Chao-Kai Shu, Wang-Lin Liu, Sol. Energy Mater. Sol. Cells 95 (2011) 1940.
[16] Sh Shen, X. Chen, F. Ren, C. X Kronawitter, S. S Mao, L. Guo, Nanoscale Res. Lett. 6 (2011) 290.
[17] M. Yousaf, M.A. Saeed, Ah R. Mat Isa, H.A. Rahnamaye Aliabad, M.R. Sahar, Chin. Phys. Lett. 30 (7) (2013) 077402.
[18] I.G. Stamov, N.N. Syrbu, V.V. Ursaki, V.I. Parvan, V.V. Zalamai, Optic Commun. 285 (24) (2012) 5198.
[19] N.N. Syrbu, A.V. Tiron, V.I. Parvan, V.V. Zalamai, I.M. Tiginyanu, Phys. B Condens. Matter 463 (2015) 88.
[20] H. Sobotta, V. Riede, Wiss. Z. Karl-Marx_Univ. Leipzig, Math,-Naturviss. R. 20 (1971) 147 ([in German]).